Development of novel clam shell-derived activated carbon by calcination and activation method for dye removal

Lia Anggresani[1,2], Mahmoud El Nouby[3], Andi Rachman[1],
Tsugufumi Matsuyama[4], Aster Rahayu[5], Lee Wah Lim[1,4*]

[1] Graduate School of Engineering, Gifu University, Yanagido 1-1, Gifu-Shi, Gifu, Japan
[2] Department of midwifery, Syedza Saintika University, Jl. Prof. Dr. Hamka, Padang City, West Sumatera, Indonesia
[3] Department of Pesticide Chemistry and Technology, Faculty of Agriculture, 21545-El-Shatby, Alexandria University, Alexandria, Egypt
[4] Department of Chemistry and Biomolecular Science, Faculty of Engineering, Gifu University, Yanagido 1-1, Gifu-Shi, Gifu, Japan
[5] Department of Chemical Engineering, Faculty of Industrial Technology, Universitas Ahmad Dahlan, Yogyakarta, 55166, Indonesia
* Corresponding author's e-mail: lim.lee.wah.u7@f.gifu-u.ac.jp

ABSTRACT

Synthetic dyes like Congo Red are commonly used in textile and batik industries, especially in Indonesia. The dyes are toxic, non-biodegradable, and pose significant environmental hazards if not treated properly prior to disposal. The removal of such dyes from aqueous solutions is feasible with conventionally activated carbon, but its expensiveness and non-renewable source at the industrial level. Clam shell waste, being rich in calcium carbonate ($CaCO_3$) content and abundantly available, presents a promising alternative precursor to produce activated carbon. The present work is focused on preparing an eco-friendly and low-cost activated carbon from waste clam shell through calcination and chemical activation with KOH. The research examines the structural modification, adsorption characteristics, and prospective applications of the resultant adsorbent in the decolorization of Congo Red dye. Clam shells were washed, dried, powdered, and calcined at 500 °C. The calcined sample was activated with KOH in molar ratios from 1:1 to 1:4. The resultant activated carbon (SAC) was characterized using XRD, XRF, FTIR, and SEM. Batch adsorption was conducted, experimenting on stirring speed, contact time, and dye concentration. Adsorption kinetics and isotherms were studied through pseudo-second-order, pseudo-first-order, Freundlich, and Langmuir models. XRD and FTIR confirmed aragonite to calcite transformation and amorphous carbon structure formation during activation. The SEM images illustrated increased porosity, especially that of SAC 1:3, which exhibited a homogeneous network pore structure. SAC 1:3 achieved maximum dye elimination efficiency (> 99%) and adsorption capacity (1.99 mg/g) with minimum contact time. Kinetic data was satisfactory with pseudo-first-order for SAC 1:2 and 1:3, with physisorption as the predominant mechanism, and SAC 1:4 fitted closer to the pseudo-second-order model with the implications of chemisorption. The Langmuir isotherm analysis indicated monolayer adsorption with both SAC 1:2 and SAC 1:3 exhibiting a maximum adsorption capacity of 1.87 mg/g. This research effectively proves the possibility of using clam shell waste as a high-performance, sustainable adsorbent to remove dyes. The optimized sample, SAC 1:3, presents a solution with much potential for water treatment purposes, particularly in areas with environmental issues caused by textile dye pollution.

Keywords: clam shell, activated carbon, calcination, activation, dye removal.

INTRODUCTION

Increasing environmental concerns due to dye-containing wastewater, particularly from textile industries, have prompted the search for effective, environmentally friendly, and low-cost adsorbents for water treatment (Aftab et al., 2024; Ali et al., 2021; Aragaw and Bogale, 2021; Crini, 2006). Among various treatment processes, adsorption has gained significant attention due to its

simplicity, efficiency, and cost-effectiveness (Sevilla and Fuertes, 2011). Because of its high surface area, porosity, and adsorption capacity, activated carbon is considered one of the most suitable adsorbents for the removal of organic pollutants such as artificial dyes like Congo Red (Tan et al., 2008).

The textile industry is one of the largest generators of industrial liquid wastewater due to its high-water demand, with approximately 100–200 tons of water used for every ton of fabric processed, 80–90% of which becomes wastewater (Kant, 2012; Yaseen and Scholz, 2019). Much of this wastewater consists of synthetic dyes that are non-biodegradable and highly stable. It is estimated that approximately 300,000 tons of dyes and corresponding pollutants are discharged annually into aquatic environments in textile and dyeing processes (Chung, 2016; Correia et al., 1994). Although Congo Red is only one type of azo dye, the simultaneous discharge of a vast array of dye types is cumulatively accountable for the overall pollutant load, so it is necessary to ascertain Congo Red's individual contribution within the framework of this bigger picture.

In Indonesia, Congo Red is utilized extensively in the batik industry, an economically and culturally important industry. Congo Red is a widely used commercial azo dye that has been extensively utilized in dyeing textiles due to its structural stability, intense red color, good fastness, and affinity of the fiber to cellulose. Congo red is classified as a mutagenic and potentially carcinogenic compound that contributes significantly to the high chemical oxygen demand (COD). Congo Red has been extensively utilized in Indonesia in the batik industry as a prominent dyeing agent (Wulansarie et al., 2023). Batik itself is not only a traditional cloth but a reflection of culture, which has been recognized by UNESCO as an Intangible Cultural Heritage of Humanity in 2009 (UNESCO Intangible Cultural Heritage, n.d.). Production of Batik involves complex wax-resist dyeing procedures and typically requires the application of synthetic dyes like Congo Red to achieve brilliant and long-lasting colors. However, wastewater discharged from batik dyeing processes contains residual dyes that are non-biodegradable, poisonous, and destructive to aquatic ecosystems if untreated (Nadhira Nasron et al., 2018).

Traditionally, activated carbon has been produced from fossil-based materials such as coal and petroleum products. Such conventional precursors are costly and environmentally unstable

(Abdullah et al., 2011; Ioannidou and Zabaniotou, 2007; Iwanow et al., 2020; Vilén et al., 2022). In the last ten years, there has been a growing tendency to utilize biowaste as a precursor material for the generation of activated carbon. Fruit peel, agricultural residues, and shell of marine animals are extremely interesting since they are easily accessible, cheap, and have a high carbon or calcium carbonate content (Ahmad et al., 2021; Ioannidou and Zabaniotou, 2007; Zhang et al., 2024a).

Among the numerous calcium-containing wastes, seashells have been selected as an activated carbon because of the following primary advantages. Marine clam shells, a calcium carbonate-derived biowaste and contain very high purity and commonly discarded by seafood processing and restaurant industries, are an underutilized resource with immense material engineering potential. Studies have in the past focused on the application of seashells in cement composites and bio-ceramics (Yoon et al., 2023), but as a precursor for activated carbon, their application is relatively untapped. Because they contain high amounts of $CaCO_3$, clam shells can be heat converted and chemically treated to produce porous carbonaceous materials (Oral et al., 2020). This study aims to develop and characterize activated carbon derived from *Ruditapes philippinarum* (Manila clam) waste using calcination and KOH activation. The resulting materials are evaluated for their structural properties and adsorption performance in removing Congo Red dye from aqueous solutions. This research contributes to sustainable biowaste valorization and offers a promising solution for environmental remediation, particularly in coastal regions with abundant shellfish waste and dye pollution.

Seashells are primarily made up of calcium carbonate ($CaCO_3$) and contain very high purity levels – typically greater than 95% – and are extremely easily available in the form of industrial seafood waste, especially by coastal regions. The global seafood industry generates tens of millions of tons of waste shells each year, which is wasted or landfilled and which causes both environmental and public health problems (Thor Sigfusson et al., 2024). Relative to other $CaCO_3$-rich waste products such as eggshells, bone char, or limestone sludge, seashells have superior thermal stability, mechanical strength, and surface morphology, and therefore are more suitable for calcination and chemical activation in high-temperature processes (Hart and Onyeaka, 2021). Moreover, their

vast abundance and low cost guarantee a green and circular waste valorization process. These characteristics make it reasonable to choose seashells as a promising raw material for the preparation of effective adsorbents for the removal of synthetic dyes from wastewater.

In Indonesia, seashell wastes are on the rise each year with increasing production of shellfish (Hamid, 2020). Indonesia's national shellfish production had totaled nearly 55,000 tons as of 2011, and recent news accounts indicate tons of shells are going unused (Purnamasari et al., 2024). For example, in one province, 12,000 tons of seashell waste were present in 2019 (Farhan, 2024). In Surabaya, the estimated production of shell waste is 12,823 tons a year, and in Ketapang village, the monthly rate is 155.5 tons (Istikharoh and Bahtiar, 2022). Gresik, which is a major seafood-processing region, had alone produced 8,065.3 tons of shell waste in 2018 (Kurniawati et al., 2023). Although part of this waste is used for handicraft or milled to calcium supplements, the majority is lost without alternative uses, contributing to environmental problems. These figures show the large and untapped seashell waste in Indonesia, further justifying its use as a green precursor to make activated carbon.

The use of potassium hydroxide (KOH) as an activating agent has been well documented to be an effective method to synthesize microporous activated carbon with tailored pore structures and enhanced surface properties (Choi and Ryoo, 2007; Hu et al., 2011a; Sevilla and Fuertes, 2011). KOH activation facilitates chemical etching and gasification reactions that promote the formation of pores and enhance surface area. Sevilla and Fuertes (2011) obtained surface areas greater than 3000 m²/g using KOH-activated carbon from renewable sources, demonstrating its great performance in gas and dye adsorption.

However, the success of this process largely depends on precursor type, calcination temperature, and KOH ratio (Afandi et al., 2024). So far, little research has exhaustively explored the effects of thermal calcination and chemical activation on clam shell-derived materials physicochemical transformation and their resultant adsorption performance. Besides, no systematic research has established the complete potential of KOH-activated carbon generated from clam shells in dye removal processes (Ha et al., 2019; Yoon et al., 2023).

Ruditapes philippinarum (Manila clam) waste was used in this study to prepare activated carbon. The shell waste is not considered because the target dye, Congo red, is commonly found in effluents of textile industries in Indonesia. This study tries to demonstrate the feasibility and global applicability of transforming locally available biowaste into effective adsorbents for pollutants of international concern and also to develop a novel activated carbon material from clam shell wastes through a combination of calcination and KOH-mediated chemical activation. The morphology, structure, and surface characteristics of the resulting carbon are characterized by XRF, XRD, SEM, and FTIR measurements. Furthermore, the adsorption performance against Congo Red dye under various experimental conditions is explored. This work not only demonstrates a sustainable pathway for biowaste valorization (Hameed and Daud, 2008; Zhao et al., 2021) but also aids in the synthesis of high-performance adsorbents for environmental remediation (Babel and Kurniawan, 2003; Tan et al., 2008).

METHODOLOGY

Materials

The clam shells used in this study were derived from *Ruditapes philippinarum* (commonly known as Manila clam or Asari in Japanese), which are widely consumed and commercially available in Japan. The experimental work was carried out from August 2024 to February 2025 in the Chemistry and Biomolecular Science Lab, Gifu University, Japan. Ultrapure water (18.2 MΩ·cm) was prepared in the laboratory using the Advantech RFS342NC water purification system (Advantech Co., Ltd., Tokyo, Japan). Chemicals and reagents employed were hydrochloric acid (1 mol/L, Fujifilm Wako Pure Chemical Corporation, Osaka, Japan), potassium hydroxide (KOH, 56.11 g/mol, Junsei Pure Chemicals Co., Ltd., Tokyo, Japan), and Congo Red dye ($C_{32}H_{22}N_6Na_2O_6S_2$, 696.66 g/mol, Fujifilm Wako Pure Chemical Corporation, Osaka, Japan). The equipment for the preparation and characterization was a Kyoei electric furnace (Model YK-15 AG Form US-18, Tajimi City, Gifu Pref., Japan), autoclave in stainless steel, oven (Sanyo MOV-112, Japan), crush mill (Crush Millser, Iwatani, Japan), sieve with 100 μm hole diameter (Sanpo Type, Merck, Japan), magnetic mixer (Eyela RCX-1000D, China) with magnetic stirring bar (ϕ5 × 15 mm), centrifuge (IEC61010-2-020,

Kubota, Japan), and UV-Vis spectrophotometer (Model UV-2550, Shimadzu, Japan).

Clam shell pre-treatment

The clam shells were washed and cleaned with running water to remove any organic tissue remaining on the surface. The shells were then washed with deionized water to eliminate any remaining impurities. The shells were placed in an oven at 110 °C for 24 hours in order to completely evaporate moisture (Dampang et al., 2021). Such pretreatment is required to eliminate natural impurities (e.g., surface debris, organic contaminants, and salts) that may inhibit pore formation or carbon structure upon activation. Similar cleaning and drying processes have been employed in previous studies to improve the physicochemical qualities and adsorptive capability of shell-derived materials (Chin et al., 2020; Kaewtrakulchai et al., 2024). The dehydrated shells were crushed into smaller pieces using a crusher (Crush Millser, Iwatani, Japan). The powder was subsequently sieved through a 100 µm mesh for homogenization of particle size. The SCR powder was subsequently calcined at 500 °C for 3 hours. 500°C temperature calcination was selected to trigger phase transition from aragonite to calcite and avoid total decomposition to CaO. This type of temperature has been universally employed in the literature to preserve the carbonate structure and enhance adsorptive properties of shell-derived materials (Martinez et al., 2024). Heating was carried out stepwise: initially at 150 °C for 15 minutes, then to 300 °C for a further 15 minutes and finally held at 500 °C for 3 hours. The powder after calcination was labeled as SCR 500 °C and used for the subsequent chemical activation process.

## KOH-Assisted chemical activation process

Potassium hydroxide (KOH, 1 M) was used as the chemical activating agent throughout this work. Calcined clam shell powder (SCR 500 °C) was mixed with KOH at various molar ratios: 1:1, 1:2, 1:3, and 1:4. Mixtures were stirred on a magnetic stirrer for 1 hour, adjusting the stirring speed and contact time to ensure adequate interaction among the activating agent and precursor material. The synthesized slurry was transferred to a stainless-steel autoclave and treated hydrothermally at 150 °C for 4 hours to enhance the reactivity of the material. The samples were further calcined at 600 °C for 2 hours after hydrothermal treatment. This was done sequentially: first calcination at 200 °C for 15 minutes, then at 400 °C for 15 minutes, and finally at 600 °C for 2 hours. Following calcination, the activated carbon was washed continuously with 1 M hydrochloric acid (HCl) and deionized water to remove impurities and residual KOH. The final product was oven-dried at 105 °C for 5 hours to fully expel moisture. The KOH-activated carbon obtained from clam shells was designated as SAC (Figure 1).

Characterization

Characterization was conducted to examine the functional groups, elemental analysis, crystal phase, surface texture, surface area, and pore structure of final materials. Raw clam shell powder (SCR) and calcined sample (SCR 500 °C) along with KOH-activated samples (SAC at varied molar ratios) were characterized through the application of several analytical tools. X-ray diffraction (XRD) was done on a Rigaku UL-TIMA IV diffractometer (Japan) using Cu Kα radiation (λ = 1.5418 Å) with a graphite monochromator and LynxEye detector, at 30 kV and 10 mA. XRD was utilized to identify the crystalline phases present in the samples before and after calcination and chemical activation. X-ray fluorescence (XRF) analysis was utilized to find out the elemental composition of the samples. XRF enabled us to find out the major as well as trace elements and an indication of changes in composition caused by thermal and chemical treatments. Fourier-transform infrared (FT-IR) spectroscopy was performed on the Spectrum 400 FT-IR/FTF-IR instrument with attenuated total reflectance (ATR) accessory in a wavenumber range of 4000–400 cm^{-1}. FT-IR was employed to identify functional groups, namely those associated with carbonate decomposition and surface functionalization of the activated carbon products. Scanning electron microscopy (SEM) SU3500 (Hitachi Ltd, Tokyo, Japan) was utilized to examine the surface morphology and structural evolution of the samples at various preparation stages. SEM on a Hitachi SU3500 instrument (Hitachi Ltd., Tokyo, Japan) was used to examine the surface morphology of samples. SEM imaging provided visual details on the development of pores, roughness of the surface, and integrity of structure at different stages of processing, i.e., raw, calcined,
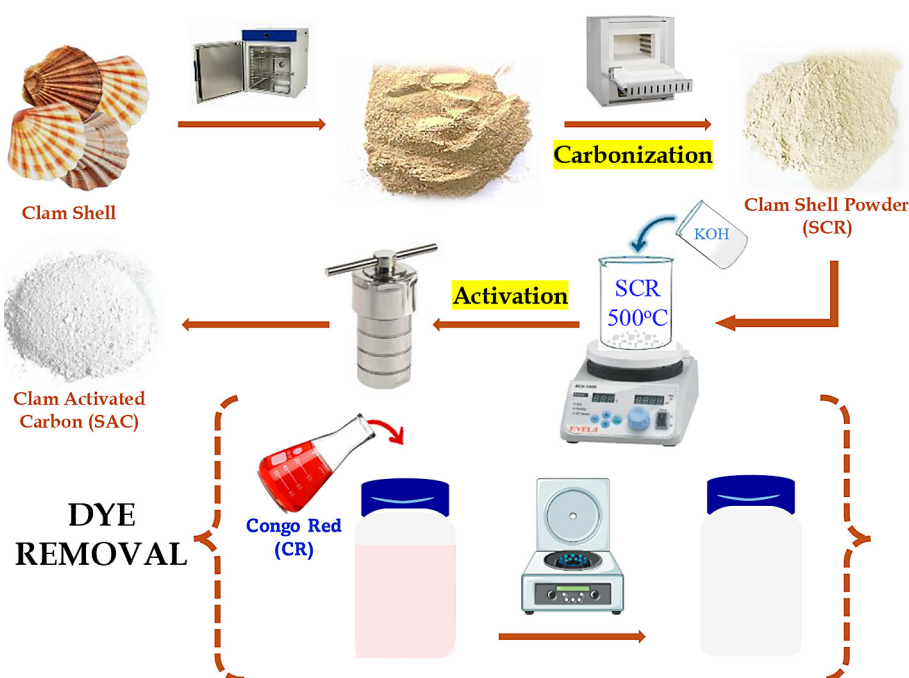
Figure 1. Flowchart of clamshell derived activated carbon by calcination and activation method

and chemically activated. It played a significant role in comprehending the development of microstructure and its relation to adsorption efficiency.

Adsorption studies

The adsorption experiment was conducted using the batch adsorption method to determine the effectiveness and adsorption capacity of sea clam shell-activated carbon (SAC) in removing Congo Red dye from water. Adsorbate solution was prepared by dissolving Congo Red dye in deionized water to have an initial concentration of 10 mg/L. 50 mg of SAC, previously prepared at various KOH molar ratios, was added to 10 mL of Congo Red solution in vial bottles. The mixture was stirred at varying speeds (300 and 600 rpm) to allow equal distribution and optimum contact between adsorbent and adsorbate. Contact time modifications were also investigated with various hours to analyze the adsorption kinetics. After the adsorption process, the solutions were centrifuged at 100 rpm for 15 minutes to remove the adsorbent from the solution. Quantitative determination of Congo Red in the supernatant was made with a UV-Vis spectrophotometer at λ max = 498 nm (Table 1).

Data analysis

To establish the adsorption mechanism of Congo Red on activated carbon prepared from clam shells (SAC), adsorption kinetics as well as isotherm models were employed in the modeling of experimental data.

Adsorption kinetics

The adsorption kinetics were studied to establish the rate-controlling steps encountered during the de-coloration of the dye (Table 2).

The kinetic model with the highest fit to the data was determined by correlation coefficient (R^2) and experimental and calculated q_e value comparison. The higher R^2 value and the more similar q_e show a better fit.

Adsorption isotherms

Isotherm modeling was used in order to consider the equilibrium relationship between the solution-borne dye and adsorbed dye. Two isotherm models were used (Table 3).

The validity of both models was determined by comparing regression coefficients (R^2). A Langmuir model suggests monolayer adsorption on an even surface, while Freundlich model suggests adsorption on an uneven surface with varying affinities.

Table 1. Adsorption parameters and definitions

Parameter	Equation
Removal efficiency (%)	$\% \ RE = \frac{C_o - C_e}{C_o} \times 100$
Adsorption capacity (q$_e$)	$q_e = \frac{(C_o - C_e) \times V}{m}$

Note: C_o is initial concentration of adsorbate (mg/L), C_e is final concentration of adsorbate (mg/L), q_e is adsorption capacity (mg/g), v is volume of solution (L), and m is weight of adsorbent (g)

RESULTS AND DISCUSSION

This study was carried out to evaluate the effectiveness of carbon activation based on clam shells-derived activated carbon (SAC) in adopting Congo red. The analysis was carried out on changes in morphology, surface area, adsorption capacity, as well as kinetic and isotherm parameters of adsorption. One of the parameters in this study is the % yield of activated carbon produced through the calcination and activation process.

Table 4 shows the yield calculation data for each sample, namely SCR 500 °C and SAC with different KOH activation ratios. In the 1:1 SAC sample, the % yield shows 27.7%. This shows that in this ratio there is a reaction between KOH and CaO, which produces dissolved or volatile compounds that are excessive due to heating and washing. In contrast to SAC 1:2–1:4, the % yield produced > 89% (Afandi et al., 2024). It is seen that the increased KOH ratio will increase the retention of the carbon life, this may be due to the

stabilization of the carbon structure and increased porosity without material loss (Hu et al., 2011b; Sevilla and Fuertes, 2011). SAC 1:1 is likely to affect the effectiveness of adsorption of textile dyes (Hameed and Daud, 2008). However, SAC with a large KOH ratio will be more optimal if applied as an adsorbent (Tan et al., 2008; Zhao et al., 2021). Further review based on the results of other analyses or characterizations like x-ray fluorescence (XRF), x-ray diffraction (XRD), SEM and fourier transform infra-red (FTIR) (Ha et al., 2019; Zhao et al., 2021).

X-ray fluorescence (XRF)

XRF analysis was carried out to determine the elements contained in clam shells (SCR), calcined clam shells 500 °C, and calcined clam shells activated with KOH with various mole ratio (SAC 1:1 - 1:4). Some of the main elements are seen in Figure 2. including calcium (Ca), potassium (K), nickel (Ni), zinc (Zn), strontium (Sr) and zirconium (Zr). At energies between 3.5–3.8 keV, the peak of Ca Kα and Ca Kβ dominates, indicating that calcium is the main element found in all samples (Buasri et al., 2013). The highest intensity can be seen in the clam shell before calcination process, which is consistent with its naturally high $CaCO_3$ content, as reported in similar biogenic material studies (Oral et al., 2020; Yoon et al., 2023). Meanwhile, the intensity significantly increases with the increasing of the ratio of KOH. This indicated that the reduced calcium content

Table 2. The general kinetic models were utilized

Parameter	Pseudo-first-order model	Pseudo-second-order model
Linear	$\log(q_e - q_t) = \log q_e - \frac{K_1}{2.303} t$	$\frac{t}{q_t} = \frac{1}{K_1 q_e^2} + \frac{t}{q_e}$
Nonlinear	$q_t = q_e(1 - e^{-k_1 t})$	$q_t = \frac{q_e^2 K_1 t}{1 + q_e K_1 t}$

Note: q_t is the amount of dye adsorbed at time t (mg/g), q_e is amount of dye adsorbed at equilibrium (mg/g), k_1 is pseudo-first-order rate constant (1/h), k_2 is pseudo-second-order rate constant (g/mg·h).

Table 3. The two isotherm models

Parameter	Langmuir isotherm	Freundlich isotherm
Linear	$\frac{C_e}{q_e} = \frac{1}{K_L q_{max}} + \frac{C_e}{q_m}$	$\log q_e = \log K_f + \frac{1}{n} \log C_e$
Nonlinear	$q_e = \frac{q_{max} \cdot K_L \cdot C_e}{1 + K_L \cdot C_e}$	$q_e = K_f \cdot C_e^{1/n}$

Note: q_e is amount of dye adsorbed at equilibrium (mg/g), C_e is equilibrium concentration of dye in solution (mg/L), q_{max} is maximum adsorption capacity (mg/g), K_L is Langmuir constant related to adsorption energy (L/mg), K_f is Freundlich constant related to adsorption capacity, 1/n is adsorption intensity.

Table 4. Percentage yield from activated carbon

Samples	Initial weight (mg)	Final weight (mg)	% yield
SCR 500 °C	10004.4	9759.6	97.6
SAC 1:1	3023.0	837	27.7
SAC 1:2	4046.0	3926.6	97.0
SAC 1:3	2023.0	1796.1	89.8
SAC 1:4	2023.2	1938.1	95.8
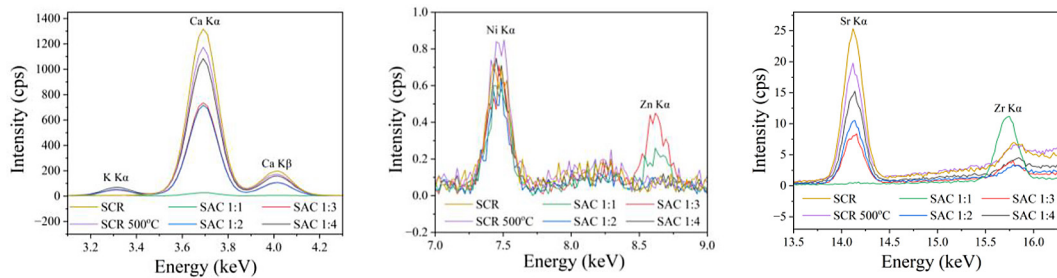
Figure 2. XRF analysis of the raw and treated samples

is due to the activation process using the KOH activator, even though the main component is Ca because the shells are rich in $CaCO_3$ content.

In Figure 2a, the peak of Ca is not visible at the SAC 1:1, but the Ca content increases as the composition of the KOH increases. Lower KOH counts result in less effective activation when retaining CaO in this activated carbon structure. During the washing process, CaO primarily reacts with KOH to form soluble compounds (Afandi et al., 2024; Sevilla and Fuertes, 2011). This can also be seen from the % yield for SAC 1:1, which is very low. By forming a porous structure through a reaction between KOH and carbon, KOH increases the surface area and porosity of activated carbon.

In addition, the presence of element K Kα is also seen in Figure 2a in the SAC 1:1 – 1:4 sample in the energy range 3.2–3.4 keV, where the peak with high intensity can be observed in SAC 1:4, while in SCR and SCR 500 °C the element K Kα is not clearly visible. The increase in K signal intensity is an indication of incorporation of potassium-containing compounds into the structure of the material due to KOH activation, as demonstrated by such similar alkali activator studies (Zhao et al., 2021). KOH can combine with CaO to create compounds like K_2CO_3 or $KCa(OH)_3$, which can make the K Kα peak stronger in XRF analysis. In the SCR and SCR 500 °C samples, it is still dominated by $CaCO_3$ because there is no addition of KOH activators. However, element K Kα may be present but in minimal amounts or in the form of low-intensity compounds so that it is not detected in XRF analysis.

In Figure 2b, the presence of the elements Ni Kα and Zn Kα at energy levels of 7.3–7.7 keV and 8.4–8.8 keV, respectively. Ni Kα was found in all samples, which could be due to pollution from the environment or a natural impurity in the shell. Its appearance during treatments reflects minimal reactivity with KOH or heat treatments, consistent with similar findings in shell-derived materials (Zhao et al., 2021). The activation process using KOH did not affect the amount of Ni Kα in any of the samples.

The presence of the element Zn Kα was not visible in the SCR and SCR 500 °C samples. This suggests that Zn Kα may have originated from interaction with KOH activators or because of impregnation during activation. In contrast to SAC 1:3, the presence of the element Zn Kα shows a higher intensity compared to SAC 1:1. This suggests that a greater amount of KOH allows for stronger interactions between Zn Kα and activated carbon, so that more Zn Kα is adsorbed in the structure of the material. At SAC 1:1, a lower amount of KOH leads to activation that is less effective in retaining Zn Kα in the activated carbon structure, resulting in a lower intensity than at SAC 1:3. This can imply incorporation or activation-related surface modification with Zn species upon KOH treatment. This kind of elemental enrichment upon chemical activation has been seen in other carbonaceous materials too (Tan et al.,

2008). However, Zn Kα undergoes further reactions with KOH at SAC 1:4 to form a compound that is more easily dissolved and released during the washing process causing it to be undetectable in XRF analysis. A phenomenon observed in excess alkali treatments (Lua and Yang, 2004).

The presence of the element Sr Kα (Figure 2c) shows high intensity in the SCR and SCR 500 °C samples in the energy range of 14.0–14.4 keV, but in the SAC 1:1 sample, the presence of the element Sr decreases dramatically or even not noticeably. This loss is most likely due to Sr volatilizing as soluble species or thermally volatilizing upon activation, similar to the behavior of Sr during thermal decomposition of carbonates in matrices (Yoon et al., 2023).

In contrast, the peak of the Zr element showed the highest intensity compared to the other samples. Further confirmation using the standard addition method is needed for confirming the Zr peak observed at the SAC 1:1 ratio to ensure it is genuinely associated with KOH activation. This is in line with previous descriptions of elemental redistribution and exposure following chemical and thermal treatment (Ha et al., 2019). In addition, activation gives rise to the redistribution of elements in the carbon matrix, which previously Zr trapped in the structure became exposed and easily detected by XRF. So that the activation carried out will not only affect the morphology and porosity of the activated carbon but also modify the composition of its constituent elements significantly (Sevilla and Fuertes, 2011; Zhao et al., 2021).

X-ray diffraction

X-ray diffraction (XRD) analysis was focused to investigate the crystalline phases present in the clam shell powder (SCR) before and after calcination at 500 °C, as well as after KOH activation at different molar ratios (SAC 1:1 – 1:4). XRD patterns obtained provide insight into the phase transformation, crystalline changes and amorphization of the material, which are crucial for its performance as adsorbent. Figure 3. presents the XRD patterns of the raw clam shell powder (SCR), calcined seaclam shell at 500 °C (SCR 500 °C) and KOH-activated carbon at different ratios (SAC 1:1 – 1:4).

Phase transformation of clam shell during calcination

The XRD pattern of the untreated seaclam shell (SCR) exhibits sharp diffraction peaks corresponding to aragonite ($CaCO_3$), which is the dominant polymorph of calcium carbonate found in marine shells (Oral et al., 2020). The presence of aragonite is confirmed by diffraction peaks at $2\theta = 26.2°$, 27.2°, 33.1°, 36.0°, and 45.9°, which are in agreement with the standard aragonite pattern (ICDD No. 00-041-1475)(Azmi et al., 2014; Islam et al., 2013). Aragonite has an orthorhombic crystal structure which gives mechanical strength of shells.

After calcination at 500 °C (SCR 500 °C), a transformation from aragonite to calcite ($CaCO_3$) was observed. This phase transition is marked by the disappearance of aragonite peaks and the appearance of new peaks at $2\theta = 29.4°$, 36.0°, 39.4°, 43.1°, and 47.5°, which correspond to the crystalline structure of calcite (Ha et al., 2019; Yoon et al., 2023). This transformation occurs because aragonite is a metastable phase that recrystallizes into calcite when subjected to moderate thermal treatment.

At higher temperatures (~700–900 °C), calcite would typically decompose into calcium oxide (CaO) through thermal decomposition:

$$CaCO_3 \rightarrow CaO + CO_2 \uparrow \qquad (1)$$

However, since the calcination temperature in this study was limited to 500 °C, the decomposition into CaO did not occur significantly. Instead, the primary transformation observed was aragonite to calcite recrystallization. Ha et
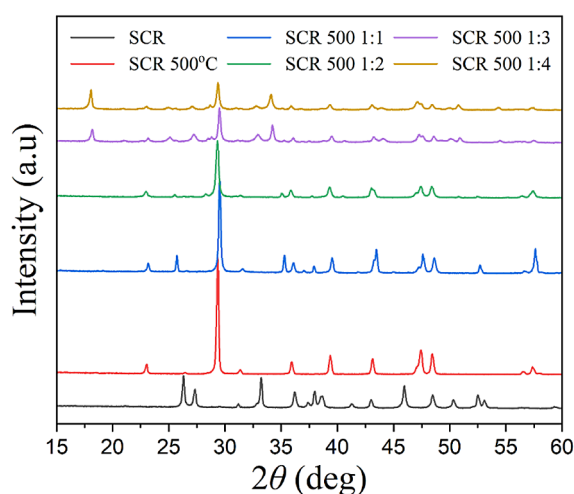
Figure 3. XRD analysis of the raw and treated samples

al reported that calcite was formed in the oyster shell with the calcination temperature at 500–700 °C (Ha et al., 2019).

Effects of KOH activation on crystalline structure

The XRD analysis of SAC 1:1-1:4 demonstrates structural altered significantly. Upon chemical activation with KOH, the intensity of calcite peaks significantly decreases, and broad amorphous humps appear, particularly in the range of $2\theta = 20$–$30°$ (Chaisit et al., 2020; Ramirez et al., 2020). These changes indicate a progressive loss of crystalline and the formation of highly porous carbonaceous material (Zhao et al., 2021). The loss of calcite peaks at SAC1:3 and SAC 1:4, indicates that the increase in KOH moles leads to increased structural irregularities and the formation of adsorbents with greater porosity.

The reduction in crystalline peaks suggests that alkaline activation partially dissolves the $CaCO_3$ phase, facilitating the formation of a more disordered carbon structure. The following reaction mechanism is proposed for the transformation during KOH activation:

$$6KOH + CaCO_3 \rightarrow 3K_2CO_3 + Ca(OH)_2 \quad (2)$$

At elevated temperatures, potassium carbonate (K_2CO_3) decomposes, contributing to the development of mesoporous and microporous structures in the activated carbon. This process enhances the surface area and adsorption capacity of the material, making it more effective for dye removal applications (Afandi et al., 2024; Zhao et al., 2021).

From Table 5 indicates the crystallographic and structural characteristics of raw and treated clam shell samples including crystallite size, crystalline, and structural description. These are very critical in establishing the effect of calcination and chemical activation on the transformation and performance of resulting activated carbon. The raw clam shell (SCR)

showed a crystallite size of 34.21 nm with high crystallinity in reference to the aragonite phase ($CaCO_3$), the natural polymorph found in seashells. The results concur with the findings of Oral et al (Oral et al., 2020), where aragonite was the dominant phase in calcium carbonate-based materials derived from biogenic sources.

After calcination at 500 °C (SCR 500 °C), the crystallite size was 36.34 nm, indicating recrystallization of aragonite to calcite. This type of phase transition is typical for calcium carbonate after moderate thermal treatment, as in oyster shell calcination studies by Ha et al (Ha et al., 2019). Chemical activation using KOH led to a remarkable decrease in crystallinity in all the SAC 1:1–1:4 samples. SAC 1:1 exhibited the first indication of amorphization, which is an indication of the commencement of disruption of crystal lattice. With higher ratios of KOH (SAC 1:2 to SAC 1:4), the structure became more disorderly, and SAC 1:3 and SAC 1:4 was most amorphous. In these samples, wide diffraction humps are observed within a range of $2\theta = 20$–$30°$ indicating that the structures are highly porous and amorphous carbon structures, typical for adsorption purposes (Nasron et al., 2018).

This structural transformation can be attributed because of the excellent chemical reaction between KOH and $CaCO_3$, which yield K_2CO_3 and $Ca(OH)_2$, favoring the development of microporous and mesoporous structures. Sevilla and Fuertes (Sevilla and Fuertes, 2011) also demonstrated that higher concentrations of KOH during activation enhance porosity and surface area, which increase adsorptive capacity. The amorphous character of SAC 1:3, in particular, points to optimal compromise between pore development and structural integrity, and as such is the most optimal for application in dye removal. Zhao et al. [(Zhao et al., 2021) demonstrated comparable findings, emphasizing the role of calcination and

Table 5. Crystallographic and structural properties of raw and treated samples

Samples	Crystallite size (nm)	Crystallinity	Structure
SCR	34.21	High crystallinity (Aragonite)	Crystalline organized
SCR 500 °C	36.34	Medium crystallinity (Calcite)	Aragonite partially degraded
SAC 1:1	35.91	Low crystallinity	First amorphization
SAC 1:2	26.55	Medium amorphous	Formation of a porous structure
SAC 1:3	30.07	High amorphous	Improve surface porosity
SAC 1:4	27.14	Maximum amorphous	Micropores

activation conditions in enhancing the adsorptive property of seashell-derived materials.

Fourier transform infra-red (FTIR)

FTIR spectroscopy was employed to investigate the functional groups present and chemical transformations occurring in raw clam shells (SCR), calcined shells (SCR 500 °C), and activated carbon products (SAC 1:1 – SAC 1:4). The FTIR spectra obtained are shown in Figure 4, and corresponding wavenumbers and their respective functional group assignments have been shown in Table 6. SCR and SCR 500 °C exhibited strong bands of absorption at 1091, 1410–1464, 873–888, and 712–725 cm^{-1}, which are each due to carbonate (CO_3^{2-}) vibrations. The 1091 cm^{-1} absorption band arises due to the symmetric stretching (v_1) of carbonate, which occurs in the aragonite polymorph of calcium carbonate, as reported by Oral et al (Oral et al., 2020). The bands between 1410–1464 cm^{-1} are of asymmetric stretching vibrations (v_3) and those between 873–888 cm^{-1} and 712–725 cm^{-1} are of out-of-plane (v_2) and in-plane (v_4) bending modes, respectively. The presence of these peaks signifies carbonate-rich nature of clam shell material prior to its activation and transformation during processing, consistent with Ha et al (Ha et al., 2019) and Yoon et al (Yoon et al., 2023) findings.

With chemical activation using KOH, the band at 1091 cm^{-1} was not observed in SAC samples, indicating the complete conversion of aragonite and breakdown of the carbonate groups with activation. This observation supports the XRD observations that revealed the transformation of aragonite to calcite and further transformation to an amorphous phase at high KOH ratios. In addition, two distinct low-wavenumber peaks at 481 and 565 cm^{-1} were present in all samples, which are assigned to Ca–O bending vibrations. Such vibrations are characteristic of biogenic calcite and aragonite and suggest that calcium-containing phases are still present, albeit in structurally modified forms (Sevilla and Fuertes, 2011; Zhao et al., 2021).

A sharp band at approximately 2342 cm^{-1} was apparent in the FTIR spectrum that was observed only for both the SCR and SCR 500 °C samples. The band is attributed to an asymmetric stretching vibration of physically adsorbed carbon dioxide (CO_2) resulting from either ambient air exposure or due to partial decomposition of $CaCO_3$. The lack of this peak in the SAC samples indicates that CO_2 was either desorbed under thermal treatment or chemically transformed into compounds like potassium carbonate (K_2CO_3) or calcium hydroxide ($Ca(OH)_2$), as reported in other activation studies (Afandi et al., 2024; Norman B. Colthup et al., 1990).

All the samples possessed weak to moderate bands in the range of 2980–2987 cm^{-1}, which are attributed to C–H stretching vibrations. These bands indicate the presence of trace organic content, perhaps because of unreacted biomass or added during KOH activation treatment. Hameed and Daud also observed such bands in activated carbon prepared from agricultural waste (Hameed and Daud, 2008). Interestingly, no intense absorption bands in the 2100–2200 cm^{-1} region were detected, which would be characteristic of triple bonds such as C≡C or N≡C. This is confirmation of the absence of alkyne or isocyanate groups in the samples, also reflecting the inorganic and carbonate-rich nature of the raw and activated samples.

More data is provided in Table 3, where the infrared absorption bands and corresponding functional group assignments of all samples are shown. In SCR and SCR 500 °C, common carbonate (CO_3^{2-}) bands such as those at 1091, 1410–1464, and 873–888 cm^{-1} are prominently observed, indicating that the aragonite and calcite structures are still dominant. The lack of 1091 cm^{-1} band in SAC samples reflects the decomposition of carbonate and transformation into amorphous form under chemical activation (Ellerbrock and Gerke, 2021; Zhu et al., 2021). The usual presence of bands at 481 and 565 cm^{-1} in every sample suggests Ca–O vibrations, but in altered
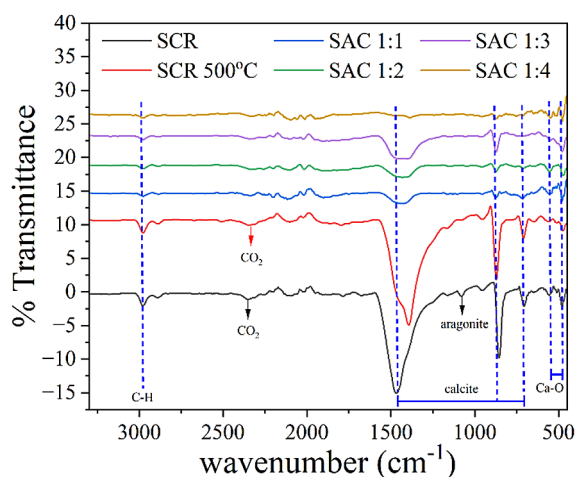
Figure 4. FTIR spectra of the raw and treated samples

Table 6. IR absorption bands and corresponding possible functional groups of raw and treated samples

Wavenumber (cm⁻¹)						Corresponding functional groups
SCR	SCR 500 °C	SAC 1:1	SAC 1:2	SAC 1:3	SAC 1:4	
481	480	484	482	483	480	Ca-O
565	566	558	562	558	552	Ca-O
710	714	725	719	714	719	CO_3^{-2} calcite
858	888	878	877	875	877	CO_3^{-2} calcite
1091	-	-	-	-	-	CO_3^{-2} aragonite
1464	1410	1443	1453	1452	1461	CO_3^{-2} calcite
2342	2348	-	-	-	-	CO_2
2986	2985	2987	2981	2981	2985	C-H (residual organic matter)

structure (Sevilla and Fuertes, 2011). The band at 2342 cm⁻¹ present only in SCR and SCR 500 °C suggests physically adsorbed CO_2, which is lost following activation by either thermal release or chemical conversion (Ioannidou and Zabaniotou, 2007). At the same time, the band at 2985 cm⁻¹ appearing in all the samples corresponds to residual organic matter (Tan et al., 2008). The absence of peaks from 2100–2200 cm⁻¹ confirms there are no triple-bond groups such as alkynes or isocyanates, which asserts the material being predominantly inorganic in nature (Coates, 2006).

Scanning electron microscope

Scanning electron microscopy (SEM) was performed to study the morphological evolution of sea clam shell-derived carbon materials at various preparation levels. The SEM micrographs of the raw clam shell powder (SCR), the calcined sample at 500 °C (SCR 500 °C), and activated carbon samples with various KOH ratios (SAC 1:1, 1:2, 1:3, and 1:4) are presented in Figure 5. The micrographs provide information on the impact of thermal and chemical treatment on surface structure and porosity.

The raw powder of sea clam shell (SCR) (Figure 5a) featured a relatively even and compact surface with minimal perceivable porosity, characteristic for biogenic forms of calcium carbonate such as calcite and aragonite (Oral et al., 2020). Calcination at 500 °C caused the surface (SCR 500 °C, Figure 5b) to be mostly cracked and exhibit formation of microcracks. It is caused by decay of organic matter and partial aragonite to calcite conversion, leading to surface integrity disruption and pore development initiation (Ha et al., 2019). More activation with KOH caused dramatic changes in morphology. For SAC 1:1

(Figure 5c), the surface exhibited initial pore formation with limited distribution, reflecting that the low KOH ratio activation begins etching the calcium-based matrix but is not effective enough for pore network formation. SAC 1:2 and SAC 1:3 samples (Figure 5d–e) exhibited high pore density and structure collapse. The surfaces became very porous, possessing irregular and broken textures, which imply extensive activation and the formation of a carbon matrix. This implies that a high to moderate ratio of KOH promotes effective chemical activation, facilitating the improvement in pore development by the redox reaction between KOH and $CaCO_3$ to create compounds such as K_2CO_3 and CO_2 that gasify the carbon framework (Sevilla and Fuertes, 2011; Zhao et al., 2021).

Among all the samples, SAC 1:3 possessed the most uniform and interconnecting porous structure, which implies the best balance of etching-structure retention. This agrees with the XRD evidence of extensive amorphization and highest surface porosity in this sample. In SAC 1:4 (Figure 5f), despite high porosity, the structure showed partial collapse, possibly due to overactivation, leading to fragility and material degradation. Over-activation with high KOH loading can potentially cause destruction of the inherent carbon structures and decrease the adsorption performance through mechanical degradation (Ioannidou and Zabaniotou, 2007).

Such morphological changes are consistent with the actual adsorption performance in batch testing, where SAC 1:3 was consistently shown to remove Congo Red more effectively, possibly due to possessing a highly accessible and porous surface. SEM confirmation affirms that both chemical activation and calcination are pivotal to structurally designing the microstructure of
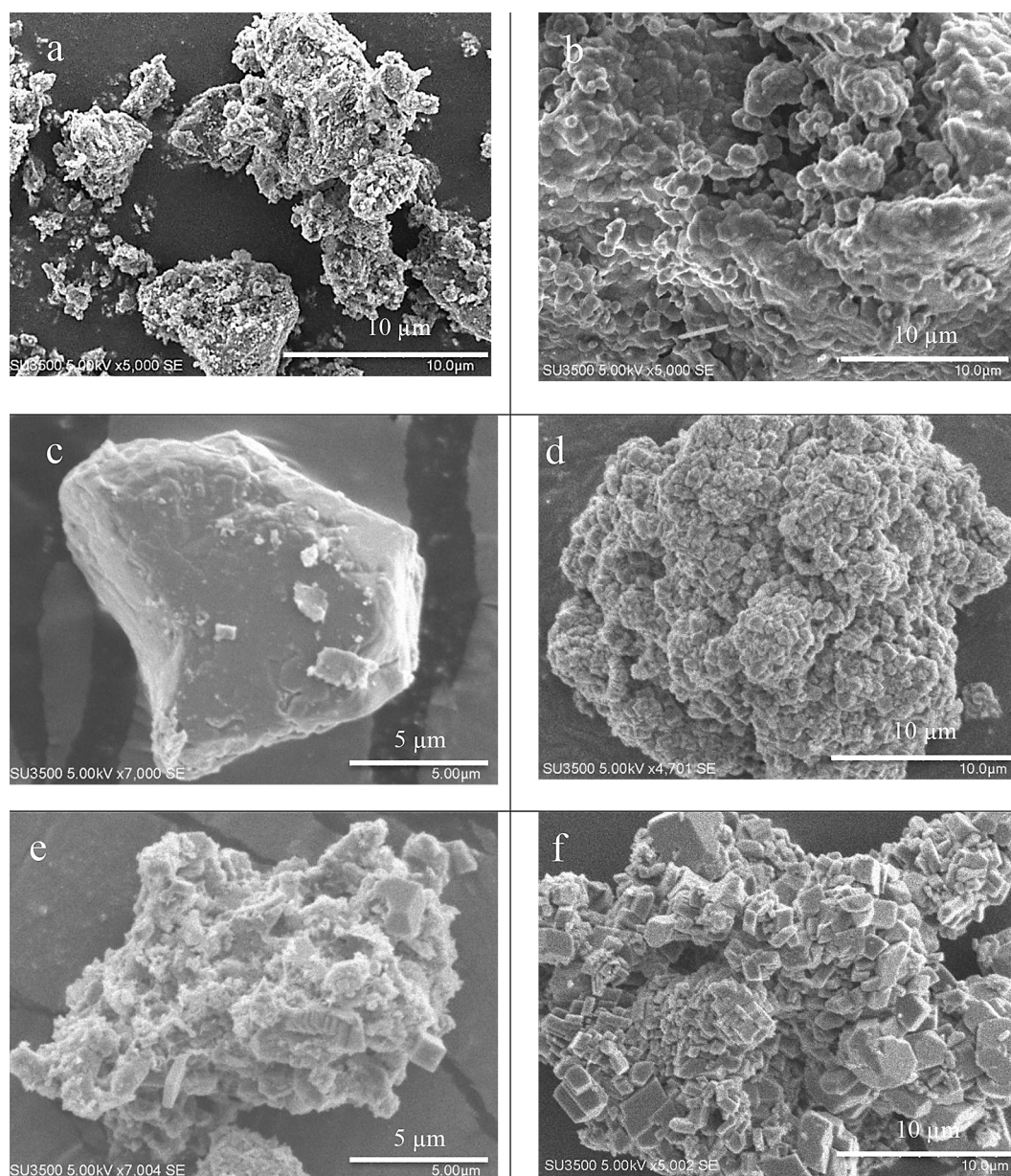
Figure 5. SEM images of the (a) SCR, (b) SCR 500 °C, (c) SAC 1:1, (d) SAC 1:2, (e) SAC 1:3, (f) SAC 1:4

carbon materials produced from biowaste, regulating their adsorption functionality.

Table 7 summarizes the average particle size and morphological characteristics observed for sea clam shell-derived samples subjected to various treatment stages, as observed using SEM analysis. The parameters provide meaningful information regarding calcination and chemical activation's impacts on the physical structure of materials, influencing surface area and adsorption capacity.

Raw clam shell powder (SCR) had the biggest particle size of approximately 1.57 µm with a comparative dense and streamlined surface. It is typical of untreated calcium carbonate-based biomaterials that, in this form, the inherent crystalline network is maintained, and porosity is low (Yoon et al., 2023). When calcined at 500 °C, the particle size reduced to 1.33 µm (SCR 500 °C). This reduction is attributed to thermal decomposition of organic residues and partial phase transformation from aragonite to calcite, which results in microfractures and degrades the particle structure (Ha et al., 2019). This initial fragmentation plays a significant role in shaping the surface accessibility of the material in the subsequent activation step.

Substantial changes were observed in the KOH-activated samples (SAC 1:1–1:4). SAC 1:1 had a particle size of 1.06 µm, indicating higher breakdown of the carbon matrix by mild chemical

Table 7. The average particle size and morphological characteristics of raw and treated materials

Samples	Average particle size (µm)	Morphology
SCR	1.57	Relatively compact dan dense structure
SCR 500 °C	1.33	Microfractures
SAC 1:1	1.06	Higher breakdown of carbon matrix
SAC 1:2	1.04	Highly porous surface with increased roughness
SAC 1:3	1.07	Homogeneous pore network
SAC 1:4	0.91	Over-etched porous structure, partial collapse

etching. However, the pore structure was still underdeveloped, i.e., the activation was not optimal at this point (Sevilla and Fuertes, 2011). Progressive decrease in the particle size with increasing KOH ratios was observed. SAC 1:2 and SAC 1:3 had particle sizes of 1.04 µm and 1.07 µm, respectively, reflecting extensive activation and surface etching that had developed a more fragmented and porous structure. Remarkably, even while SAC 1:3 possessed a relatively bigger average particle size compared to SAC 1:2, SEM images demonstrated that it had a more advanced and homogeneous pore network, demonstrating the presence of an optimum equilibrium between structure solidity and pore formation (Zhao et al., 2021).

The best particle size was recorded in the SAC 1:4 sample and was 0.91 µm. This means that over-activation leads to excessive breakdown of the structure and thus may ruin the mechanical stability of the adsorbent. While smaller particles would generally provide larger surface area, over-activation will also lead to collapse of micropores or formation of unstable frameworks (Lua and Yang, 2004). These particle size values are consistent with the SEM results and trends in adsorption performance. Optimal balance between particle size reduction and morphological stability was realized with SAC 1:3, which showed both adequate fragmentation and well-structured pore structure, thereby demonstrating itself to be a good candidate for application as an effective adsorbent in dye removal.

Adsorption studies

In the first phase of this study, activation processes were carried out on various precursor ratios to obtain activated carbon samples (SAC). Among the generated samples, SAC 1:1 performed very poorly with a yield of merely 27.7% in relation to the initial precursor mass. This very low yield indicated that a large amount of the precursor material was lost on activation, implying a grossly disproportionate amount of raw material and experimental effort would be required to produce significant amounts of SAC 1:1 for analysis.

In addition, early characterization of SAC 1:1 revealed relatively underdeveloped pore structures and surface morphology relative to other samples. These findings suggested suboptimal activation efficiency, which is likely to adversely impact its adsorption performance. In view of these factors, extremely low yield, inadequate development of pores, and unfavorable prospects of effective adsorption SAC 1:1 was excluded from subsequent adsorption experiments, kinetic investigations, and isotherm modeling. Instead, scientific endeavor was focused on SAC 1:2, SAC 1:3, and SAC 1:4, which were characterized by better yields, more developed porous structures, and favorable prospects as effective adsorbents.

From Table 8. The adsorption capacities of SAC 1:2, SAC 1:3 and SAC 1:4 was compared in terms of removal efficiency (% RE) and adsorption capacity (q_e) at two agitation speeds, 300 rpm and 600 rpm, at various contact times. SAC 1:2 exhibited consistently high removal efficiencies under both agitation speeds. At 300 rpm, %RE values above 95% were achieved in only 1 hour, and the maximum values of %RE were 98.88% at 1 hour and 98.21% at 72 hours. Adsorption capacity (q_e) was about to be constant at 1.96–1.98 mg/g at 1–2 hours, as a repeat affirmation of quick achievement of equilibrium conditions, in agreement with previous studies that well-developed porous structures attain quick adsorption equilibrium (Foo and Hameed, 2010). Slightly higher kinetics were observed for 600 rpm for SAC 1:2 with %RE values greater than 96% in 2 hours. However, a moderate decrease in %RE from 48 to 144

Table 8. Effect of stirring speed on % removal and adsorption capacity (q_e) of SAC 1:2, 1:3 and 1:4 at various contact times

Samples	Stirring speed (rpm)	Contact time (min)	% removal	Adsorption capacity (q_e) mg/g
SAC 1:2	300	0	0	0
		1	98.88	1.98
		2	93.83	1.88
		3	95.45	1.91
		4	97.92	1.96
		5	98.11	1.96
		6	95.83	1.92
		7	99.16	1.98
		48	95.45	1.91
		72	98.21	1.96
	600	0	0	0
		1	98.02	1.96
		2	98.11	1.96
		3	97.26	1.94
		4	92.97	1.86
		5	96.97	1.94
		6	98.4	1.97
		7	96.78	1.94
		24	96.88	1.94
		30	95.64	1.91
		48	87.54	1.75
		96	89.35	1.79
SAC 1:3	300	0	0	0
		1	99.07	1.98
		2	98.88	1.98
		3	94.21	1.88
		4	98.97	1.98
		5	99.26	1.99
		6	98.11	1.96
		24	94.59	1.89
	600	0	0.00	0.00
		1	97.92	1.96
		2	96.11	1.92
		3	95.64	1.91
		4	99.07	1.98
		5	93.73	1.87
		6	97.83	1.96
		7	97.83	1.96
		24	89.83	1.80
		48	90.02	1.80
		96	93.26	1.87
		144	95.64	1.91

hours would be attributed by desorption or re-equilibration phenomena under prolonged stirring, as also shown in previous works (de Luna et al., 2013; Ho and Mckay, 1999).

SAC 1:3 showed superior adsorption, particularly at 300 rpm. The efficiencies of removal were more than 99% after 5 hours, with the %RE reaching as high as 99.26%. q_e values leveled at 1.96–1.99 mg/g 600 rpm, where at a high %RE of as much as 97.83% was realized within 7 hours, later reduced slightly to 93.26% after 96 hours before further reduction to 95.64% after 144 hours. Because of the nature of the observed oscillations, this behavior suggests that SAC 1:3 possesses a highly open porous structure with rapid adsorption capability due to reduced diffusion resistance (Thommes et al., 2015). However, the same open structure likely renders the material prone to desorption upon prolonged agitation, as has been reported for porous adsorbents with more extensive pore networks (Sajjadi et al., 2019; Wang and Guo, 2020).

SAC 1:4 exhibited lower initial adsorption capacity at 300 rpm than SAC 1:2 and SAC 1:3, with %RE values starting at 88.50% and gradually increasing to 99.07% at 48 hours. Adsorption capacity at 300 rpm was between 1.65 and 1.98 mg/g. At 600 rpm, SAC 1:4 had better kinetics, and %RE values in excess of 95% were achieved in 3 hours, and good adsorption capacities (about 1.90–1.97 mg/g). A reduction to 89.26% was observed at 144 hours, suggesting that prolonged agitation may affect the stability of the adsorbed species, potentially by desorption mechanisms or mechanical deformation of the adsorbent-adsorbate interaction (Boparai et al., 2011; Gupta and Suhas, 2009; Hubbe et al., 2019).

Generally, SAC 1:3 displayed the best performance among the three highest %RE and q_e values in shorter durations of time, particularly under intermediate stirring rates (300 rpm). SAC 1:2 too underwent intensive and stable adsorption behavior, while SAC 1:4, although capable of achieving high %RE, registered longer contact durations to achieve equilibrium, particularly under low stirring rates.

Data analysis

Adsorption kinetics

The adsorption kinetics of Congo Red dye on activated carbon derived from sea clam shell (SAC) was investigated by fitting the experimental data with the nonlinear pseudo-first-order (PFO) and pseudo-second-order (PSO) kinetic model equations. Nonlinear modeling was also given preference over linearization transformation to avoid introducing bias and errors by it and distorting the intrinsic kinetic behavior, especially at low or high concentrations [24].

The kinetic parameters obtained through nonlinear regression including adsorption capacity (q_e), PFO rate constants (k_1) and PSO rate constant (k_2) and correlation coefficients (R^2) are presented in Table 9. The results show that, at a stirring speed of 300 rpm, SAC 1:2 and SAC 1:3 had good agreement with the PFO model with R^2 of 0.997. The q_e values obtained using the PFO model (1.94 mg/g for SAC 1:2 and 1.95 mg/g for SAC 1:3) were very close to the experimental values, which proves that the adsorption process is primarily governed by physisorption mechanisms (Kajjumba et al., 2018). On the other hand, SAC 1:4 had a lower R^2 value (0.959) in the PFO

Table 9. Nonlinear kinetic parameters of pseudo-first-order and pseudo-second-order models for congo red adsorption onto SAC samples at different stirring rates

Non-linear adsorption kinetics	Symbols	Units	SAC 1:2		SAC 1:3		SAC 1:4	
			300 rpm	600 rpm	300 rpm	600 rpm	300 rpm	600 rpm
Pseudo-first-order (PFO)								
Adsorption capacity	q_e	mg/g	1.94	1.9	1.95	1.9	1.76	1.9
PFO rate constant	K_1	1/h	1.5×10^7	6207.6	367910.7	172.5	5999091.7	4.19
R-square	R^2	-	0.997	0.983	0.997	0.988	0.959	0.983
Pseudo-second-order (PSO)								
Adsorption capacity	q_e	mg/g	1.94	1.89	1.94	1.9	1.8	1.89
PSO rate constant	K_1	g/mg.h	3.9×10^{10}	1×10^{-23}	1.9×10^{24}	3.6×10^{44}	8.20665	1.3×10^{16}
R-square	R^2	-	0.997	0.982	0.996	0.988	0.962	0.982

model, indicating the physical adsorption mechanism was less dominant in this case. The variation might be caused by the greater activation ratio, which might have added some additional surface functional groups that might participate in chemical interaction.

When the stirring rate was increased to 600 rpm, there was a slight reduction in the goodness of fit for the PFO model, particularly for SAC 1:2 (R^2 = 0.983). Although increased agitation enhances the external mass transfer, it may also cause disturbance of the adsorption equilibrium at the surface and therefore slightly affect the adsorption kinetics (Azizian, 2004). In contrast, the PSO model also provided excellent fits for experimental data for both samples and agitation speeds. At less than 300 rpm, the PSO model provided R^2 values of 0.997 for SAC 1:2 and 0.996 for SAC 1:3, implying that chemisorption processes, for instance, electron sharing or covalent bonding, are also present in addition to physisorption (Hubbe et al., 2019). For SAC 1:4, the PSO model provided a slightly higher R^2 value (0.962) than that of the PFO model, suggesting a greater contribution of chemisorption in this sample.

Interestingly, when the PSO model was still at 600 rpm, it retained high R^2 values (> 0.982) for all samples, highlighting the mechanism of adsorption being robust even under intensified agitation. SAC 1:4 exhibited improved kinetic fit to the PSO model at 600 rpm (R^2 = 0.982), favoring the hypothesis that surface activation increases the intensity of chemical interactions, as previously discovered with activated carbons possessing higher oxygenated functionalities (Wu et al., 2009). Generally, the comparison between PFO and PSO models shows that for SAC 1:2 and SAC 1:3, Congo Red adsorption is dominated primarily by physisorption processes with rapid external diffusion and surface buildup. It is a case of mixed mechanism for SAC 1:4 wherein chemisorption dominates increasingly at elevated stirring rates.

The experimental and modeled adsorption kinetics of Congo Red adsorption on SAC 1:2, SAC 1:3, and SAC 1:4 at different stirring rates (300 rpm and 600 rpm) are presented in Figure 6. The figures indicate the pseudo-first-order (PFO) and pseudo-second-order (PSO) model nonlinear fits. At 300 rpm, all samples have a fast adsorption of Congo Red in the initial few hours, followed by a plateau region where equilibrium is reached. Both the PFO and PSO models were able to capture the fast initial adsorption phase. However, as can be seen on closer inspection, in the case of SAC 1:2 and SAC 1:3, the PFO model offers a superior graphical representation of the experimental data, especially in the early region. The observation is consistent with the high R^2 values of the nonlinear fitting results tabulated in Table 9, where PFO fitting was found to perform better than PSO fitting for SAC 1:2 and SAC 1:3. For SAC 1:4 at 300 rpm, the kinetic curve is slightly different from the ideal fit in the PFO model, whereas the PSO model fits the experimental points more accurately, particularly at longer times. This suggests a greater contribution of chemisorption mechanisms for SAC 1:4, which is consistent with its slightly better PSO fitting performance (R^2 = 0.962 compared to R^2 = 0.959 for PFO) as reported in Table 9.

At a greater stirring speed of 600 rpm, all the samples exhibit an even faster rate towards equilibrium, typically within the first hour. This can be attributed to higher external mass transfer rates due to more agitation, which facilitates the migration of dye molecules towards the surface of the adsorbent (Azizian, 2004). While the kinetics are faster, the curves of adsorption are pretty much similar between the PFO and PSO models, indicating that the inherent mechanism of adsorption wasn't significantly influenced by increased agitation. However, a slight improvement in the fitting quality of the PSO model is observed for SAC 1:4 at 600 rpm, further reinforcing the role of chemisorption for highly activated samples. This behavior is consistent with the findings of Tan et al.(Tan et al., 2008), who reported that highly activated carbon surfaces with more oxygen-containing groups favor chemical adsorption interactions at higher agitation rates.

The similarity between PFO and PSO fitting curves for SAC 1:2 and SAC 1:3 across both stirring rates supports the conclusion that their adsorption processes are dominated by physisorption mechanisms, involving weak van der Waals forces rather than strong chemical bonds (Hubbe et al., 2019). Thus, the kinetic curves in Figure 6 graphically validate the kinetic model fitting results above and emphasize the impact of both stirring speed and activation ratio on SAC material adsorption properties.

Adsorption isotherms

The adsorption process of Congo Red (CR) on activated carbon from sea clam shell (SAC) was further investigated by applying Langmuir
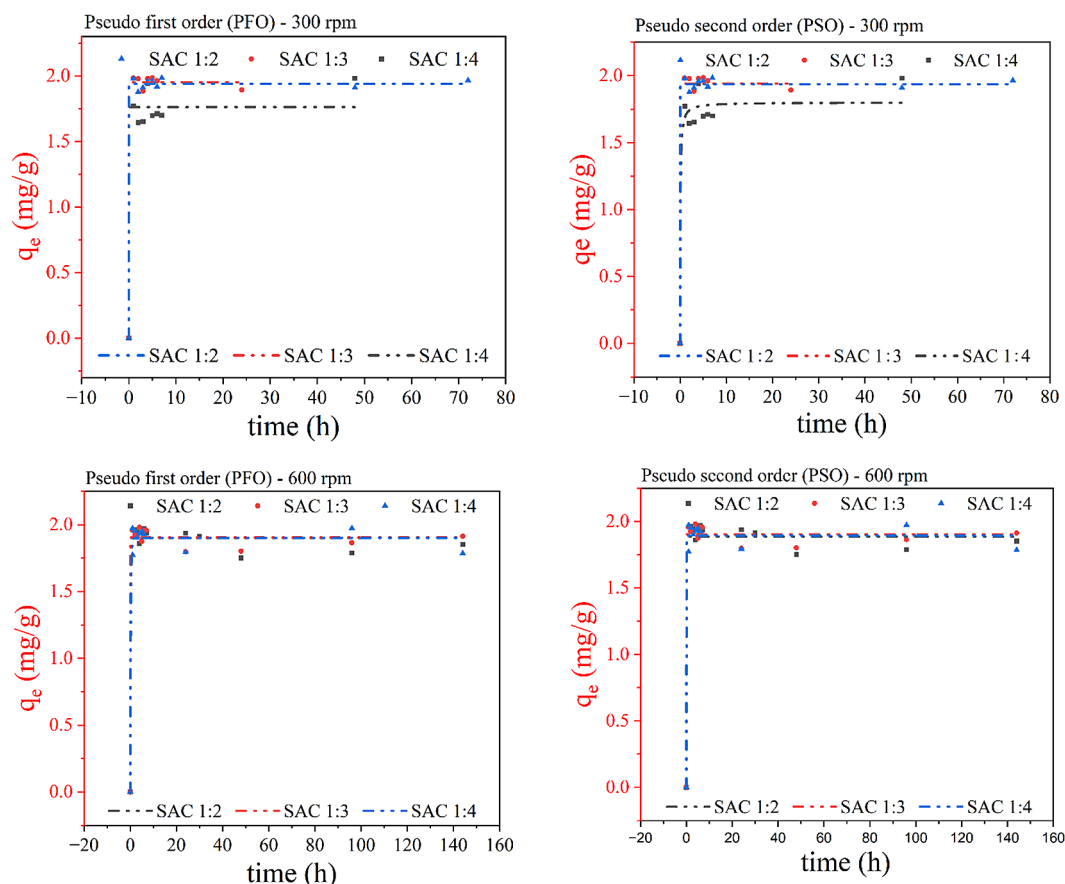
Figure 6. Nonlinear pseudo-first-order and pseudo-second-order kinetic models for Congo red adsorption onto SAC samples (SAC 1:2, SAC 1:3, and SAC 1:4) at stirring rates of 300 rpm and 600 rpm

and Freundlich isotherm models, with linearized plots provided in Figure 7 and corresponding parameters tabulated in Table 10. The Langmuir isotherm assumes monolayer adsorption onto a surface that has a finite number of homogeneous, similar sites, proposing surface homogeneity characteristics of the adsorbent (Crini and Lichtfouse, 2019). As can be seen from Table 10 the Langmuir straight-line plots yielded excellent correlation coefficients ($R^2 \approx 0.999$ for all SAC ratios at both 300 rpm and 600 rpm), which strongly supports that the adsorption of Congo Red onto SAC followed the Langmuir model under the studied conditions. This outcome is in line with Tan et al (Tan et al., 2008) and Kwiatkowski et al (Kwiatkowski et al., 2019), who reported that activated carbons possessing a developed porous structure normally exhibit Langmuir adsorption behavior due to their comparably homogeneous adsorption sites.

The greatest adsorption capacities (q_m) of the Langmuir model were 1.87 mg/g for SAC 1:2 and SAC 1:3 at 300 rpm, which decreased slightly to

1.735 mg/g and 1.77 mg/g, respectively, at 600 rpm. This slight reduction may be attributed to enhanced agitation disrupting the adsorption equilibrium, as noted by Azizian (2004). In comparison, SAC 1:4 exhibited lower q_m values (1.64–1.74 mg/g), suggesting that SAC 1:2 and SAC 1:3 possess more favorable pore structures and surface chemistry for CR adsorption, consistent with the SEM and BET results reported previously (Sevilla and Fuertes, 2011; Zhao et al., 2021).

The Freundlich isotherm, on the other hand, is a model for multilayer adsorption on non-uniform surfaces (Sevilla and Fuertes, 2011). The Freundlich model R^2 values were lower than Langmuir, that is, for SAC 1:2 and SAC 1:3, which indicates the adsorption surface was relatively homogeneous. However, for SAC 1:4, Freundlich model was a better fit compared to Langmuir at 600 rpm ($R^2 = 0.9754$ versus 0.9627), indicating higher KOH activation resulted in a more heterogeneous surface structure, leading to multilayer adsorption behavior (Babel and Agustiono Kurniawan, 2003; Tan et al., 2008).

Table 10. Linear Langmuir and Freudlich isotherm parameters for congo red adsorption onto SAC samples at different ratio and stirring speeds

Linear adsorption isotherms	Symbols	Units	SAC 1:2		SAC 1:3		SAC 1:4	
			300 rpm	600 rpm	300 rpm	600 rpm	300 rpm	600 rpm
Langmuir isotherm								
Max. ads. capacity	q_{max}	mg/g	1.87	1.735	1.87	1.77	1.64	1.74
Langmuir constant	K_1	L/mg	-123.7	-32.83	-166.7	-42.6	-23.6	-37.8
R-square	R^2	-	0.999	0.999	0.999	0.999	0.997	0.999
Freundlich isotherm								
Adsorption Intensity	n	-	-0.027	-0.054	-0.027	-0.042	-0.063	-0.052
Freundlich constant	K_f	-	1.87	1.81	1.86	1.83	1.74	1.8
R-square	R^2	-	0.938	0.928	0.967	0.885	0.907	0.929
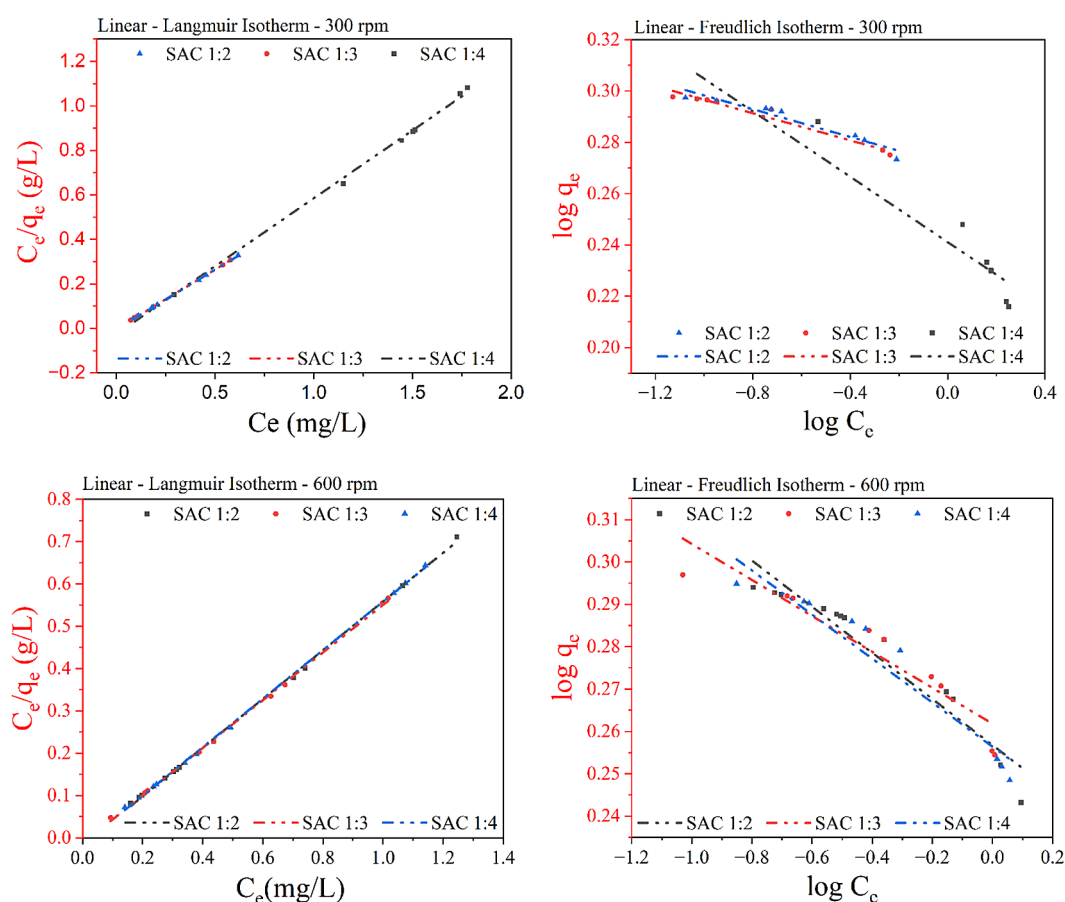
Figure 7. Langmuir and Freundlich adsorption isotherms for Congo Red dye using SAC with different ratios (1:2, 1:3, and 1:4) at 300 rpm and 600 rpm

The Freundlich constants (K_f) are capacity for adsorption, while 1/n values are intensity for adsorption [6]. However, in this study, the linearized Freundlich plots yielded negative n values (–0.027 to –0.063), which are physically less meaningful and indicate that the Freundlich model was not a good fit for describing Congo Red adsorption on SAC. This further supports the Langmuir model as more appropriate.

Meanwhile, the Langmuir qmax values slightly decreased at higher agitation speeds (e.g., SAC 1:2 from 1.87 to 1.735 mg/g and SAC 1:3 from 1.87 to 1.77 mg/g), except for SAC 1:4, which slightly increased (1.64 to 1.74 mg/g). This suggests that while higher stirring may enhance dye–adsorbent contact, it can also disrupt adsorption equilibrium, consistent with the explanation of Wu et al. (2009).

Generally, the Langmuir model better described Congo Red adsorption onto SAC samples at both 300 and 600 rpm, with particularly high correlation and adsorption capacities for SAC 1:2 and SAC 1:3 (q_m = 1.87 mg/g at 300 rpm). This indicates that monolayer adsorption predominated, consistent with relatively homogeneous adsorption sites generated through suitable calcination and KOH activation (Afandi et al., 2024; Sevilla and Fuertes, 2011). These results reinforce that preparation parameters – especially the KOH ratio and agitation rate – play a crucial role in determining the structural and adsorptive properties of SAC, and thereby its overall efficiency toward model dyes such as Congo Red (Ioannidou and Zabaniotou, 2007; Zhang et al., 2024a).

Adsorption mechanism of activated carbon derived from clam shell

The physisorption and chemisorption mechanisms are involved in the adsorption mechanism of activated carbon synthesized using clam shell as shown in Figure 8. The forces that lead to the interaction between molecules of the dye and the surface of activated carbon are many, such as π-π interactions, hydrogen bonding, and electrostatic interaction. In the physisorption region, interactions of the dye molecules with the conjugated surface carbon of the activated carbon. These are reversible and non-covalent interactions and are typically associated with weak van der waals forces (Liu et al., 2020). The planar aromatic nature of the dye permits it to stack parallel to the carbon surface and therefore can experience π-π stacking (Janekarn et al., 2020; Wang et al., 2021). Hydrogen interactions between the functional groups of the dye (e.g., $-NH_2$ and $-SO_3^-$) and the oxygen group functionalities (e.g., -OH and -COOH) on the surface of the activated carbon are also cited (Foo and Hameed, 2010; Tan et al., 2015). The bonds further stabilize the adsorption of the dye molecule and contribute to enhanced adsorption capacity (Li et al., 2003).

In the chemisorption region, electrostatic interactions are significant. The negatively charged sulfonate groups ($-SO_3^-$) of the dye molecules are attracted towards the positively charged protonated adsorbent surface functional groups or the calcium ions (Ca^{2+}) (Lim et al., 2021). Besides, the presence of potassium carbonate (K_2CO_3) and

other basic surface sites allows for stronger ionic attractions leading to a more permanent type of adsorption (Fan et al., 2018).

Environmental feasibility of using clam shell waste for dye adsorption

The use of clam shell waste as activated carbon precursor offers notable environmental advantages that are consistent with the principles of waste valorization and green materials engineering (Zhang et al., 2024b). *Ruditapes philippinarum* (Manila clam) is mostly consumed in Japan, and it generates enormous quantities of shell waste that are disposed of traditionally in landfill or through incineration (Abe et al., 2015). This waste not only contributes to contamination of the environment and to odor issues but is also a significant squandering of biogenic calcium carbonate-rich waste materials. The utilization of this waste as a valuable adsorbent addresses the double issue of waste reduction and environmental remediation.

The method used in this work demonstrates ecologically friendly pathways for material conversion (Heidarinejad et al., 2020). 500 °C calcination temperature and chemical activation using potassium hydroxide (KOH) are relatively low compared to conventionally activated carbon synthesis, where pyrolysis at extremely high temperatures over 800 °C is the general approach. Such lowered energy inputs contribute to reducing the overall carbon footprint of the material preparation process. No toxic solvents or heavy metals were employed in the synthesis, either, making the method suitable for green chemistry approaches.

Practically, from an application perspective, the SAC 1:3 sample of shell-derived activated carbon had very good performance in Congo red dye removal with the removal efficiency of over 99% after a short contact time. This indicates that shell waste products could be applied as cost-effective, renewable, and effective adsorbents for organic dye contaminants, especially in textile wastewater treatment systems. Introduction of such materials into industrial treatment units could offer an inexpensive approach to developing countries with high shellfish consumption but low availability of high-performance adsorbents (Khan et al., 2022).

In summary, the valorization of bio-waste clam shells not only minimizes the
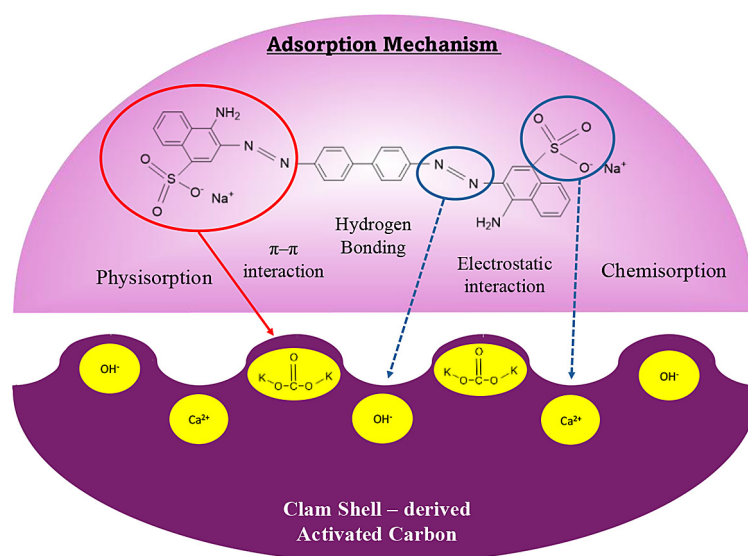
Figure 8. Adsorption mechanism of clam shell-derived activated carbon

environmental impact of biowaste disposal but also provides a sustainable approach for the synthesis of porous adsorbents for dye wastewater treatment. This research is beneficial for the eventual application of shell-based adsorbents in wastewater treatment, particularly in coastal regions where seafood waste is abundant and dyestuff pollution is a significant concern (Stefi and Vorgias, n.d.).

CONCLUSIONS

This work successfully synthesized a novel activated carbon material from sea clam shells through the combination of thermal calcination and chemical activation using potassium hydroxide (KOH). The research thoroughly studied the material's morphological, structural, chemical, and adsorption properties, with a particular focus on its application for the removal of Congo Red dye from aqueous solutions. Calcination at 500°C easily converted the aragonite phase of raw clam shells to calcite, and further KOH activation induced significant structural alterations, including the creation of amorphous carbon structures and porosity (Heidarinejad et al., 2020). Among the different activation ratios studied (SAC 1:1, SAC 1:2, SAC 1:3, and SAC 1:4), SAC 1:2 and SAC 1:3 exhibited improved physicochemical properties, with better yield, well-developed porous morphology, and significantly enhanced surface areas. Conversely, SAC 1:1 was not deeply analyzed due

to its extremely low yield and ill-developed pore structure, indicative of suboptimal activation.

XRD, XRF, FTIR, and SEM analyses all confirmed that increased KOH ratios promoted the formation of microporous structures and were accountable for enhanced adsorption performance. The SAC 1:3 sample, for instance, exhibited a highly homogeneous and well-interconnected pore network, leading to rapid dye uptake and high removal efficiency. Adsorption experiments indicated that SAC 1:3 yielded maximum removal efficiency (> 99%) and adsorption capacity (up to 1.99 mg/g) within a short contact time under moderate stirring conditions. The pseudo-first-order kinetics indicated that adsorption processes of SAC 1:2 and SAC 1:3 were pseudo-first-order, which indicated that physisorption was the dominant interaction between dye molecules and the activated carbon surface (Lima et al., 2015). For SAC 1:4, the pseudo-second-order model was more suitable, which revealed a greater extent of chemisorption processes.

Analysis of the isotherms showed that adsorption of Congo Red on SAC 1:2 and SAC 1:3 followed the Langmuir model, establishing the formation of monolayer adsorption on relatively homogeneous surfaces. SAC 1:4, however, exhibited a superior fit for the Freundlich model under certain conditions, which demonstrated a heterogeneous surface of adsorption because of over-activation (Sime et al., 2023). The resulting materials, particularly SAC 1:3, show excellent promise as renewable, low-cost adsorbents for the removal of organic dyes from wastewater. The findings represent a significant contribution to environmental

remediation and biowaste valorization and present an exciting pathway to the creation of environmentally friendly adsorbent material.

Future research would include exploring the potential for regeneration and recycling of the synthesized activated carbon to examine its long-term application. Also, employing actual industrial wastewater and other pollutants such as heavy metals or mixed dyes as adsorbents would further examine its applicability. Scaling up the preparation process and cost–benefit analyses would also further enable its commercial or industrial utilization.

Acknowledgements

REFERENCES

1. Abdullah, M. O., Tan, I. A. W., Lim, L. S. (2011). Automobile adsorption air-conditioning system using oil palm biomass-based activated carbon: A review. *Renewable and Sustainable Energy Reviews 15*(4), 2061–2072. https://doi.org/10.1016/j.rser.2011.01.012

2. Abe, H., Hasegawa, N., Yoon, S., Kishi, M. J. (2015). Evaluation of Manila clam (*Ruditapes philippinarum*) growth and microphytobenthos resuspension in a subarctic lagoon in Japan. *Hydrobiologia*, *758*(1), 87–98. https://doi.org/10.1007/s10750-015-2275-4

3. Afandi, N., Satgunam, M., Mahalingam, S., Manap, A., Nagi, F., Liu, W., Johan, R. Bin, Turan, A., Wei-Yee Tan, A., Yunus, S. (2024). Review on the modifications of natural and industrial waste CaO based sorbent of calcium looping with enhanced CO_2 capture capacity. *Heliyon 10*(5). Elsevier Ltd. https://doi.org/10.1016/j.heliyon.2024.e27119

4. Aftab, R. A., Yusuf, M., Ahmad, F., Danish, M., Zaidi, S., Vo, D. V. N., Nguyen, A.-T., Rahman, M. M., Ibrahim, H. (2024). Green technology approach towards the removal of heavy metals, dyes, and phenols from water using agro-based adsorbents: A review. *Chemistry – An Asian Journal*. https://doi.org/10.1002/asia.202400154

5. Ahmad, A. A., Al-Raggad, M., Shareef, N. (2021). Production of activated carbon derived from agricultural by-products via microwave-induced chemical activation: a review. *Carbon Letters*, *31*(5), 957–971. https://doi.org/10.1007/s42823-020-00208-z

6. Farhan, A. (2024, September 4). *Pengolahan Limbah Cangkang Kerang Sebagai Sumber Kalsium yang Bermanfaat Sebagai Sumber Mineral dan Memiliki Nilai Ekonomis Produk.*

7. Ali, K., Javaid, M. U., Ali, Z., Zaghum, M. J. (2021). Biomass-derived adsorbents for dye and heavy metal removal from wastewater. *Adsorption Science and Technology 2021*. Hindawi Limited. https://doi.org/10.1155/2021/9357509

8. Aragaw, T. A., Bogale, F. M. (2021). Biomass-based adsorbents for removal of dyes from wastewater: A review. *Frontiers in Environmental Science 9*. Frontiers Media S.A. https://doi.org/10.3389/fenvs.2021.764958

9. Hamid, A. (2020, October 8). *KKP dorong pemanfaatan kerang sebagai komoditas berdaya saing tinggi*. Antara Kantor Berita Indonesia.

10. Azizian, S. (2004). Kinetic models of sorption: A theoretical analysis. *Journal of Colloid and Interface Science*, *276*(1), 47–52. https://doi.org/10.1016/j.jcis.2004.03.048

11. Azmi, N., Yusuf, S., Sabil, K. M. (2014). Characterization and assessment of cockle shell as potential co2 adsorbents. *Applied Mechanics and Materials*, *625*, 685–689. https://doi.org/10.4028/www.scientific.net/AMM.625.685

12. Babel, S., Agustiono Kurniawan, T. (2003). Low-cost adsorbents for heavy metals uptake from contaminated water: a review. *Journal of Hazardous Materials 97*.

13. Boparai, H. K., Joseph, M., O'Carroll, D. M. (2011). Kinetics and thermodynamics of cadmium ion removal by adsorption onto nano zerovalent iron particles. *Journal of Hazardous Materials*, *186*(1), 458–465. https://doi.org/10.1016/j.jhazmat.2010.11.029

14. Buasri, A., Chaiyut, N., Loryuenyong, V., Worawanitchaphong, P., Trongyong, S. (2013). Calcium oxide derived from waste shells of mussel, cockle, and scallop as the heterogeneous catalyst for biodiesel production. *The Scientific World Journal*, *2013*. https://doi.org/10.1155/2013/460923

15. Chaisit, S., Chanlek, N., Khajonrit, J., Sichumsaeng, T., Maensiri, S. (2020). Preparation, characterization, and electrochemical properties of KOH-activated carbon from cassava root. *Materials Research Express*, *7*(10). https://doi.org/10.1088/2053-1591/abbf84

16. Chin, K. L., Lee, C. L., H'ng, P. S., Rashid, U., Paridah, M. T., Khoo, P. S., Maminski, M. (2020). Refining micropore capacity of activated carbon derived from coconut shell via deashing post-treatment. *Bioresources*, *15*(4), 77497769.

17. Choi, M., Ryoo, R. (2007). Mesoporous carbons with KOH activated framework and their hydrogen adsorption. *J. Mater. Chem.*, *17*(39), 4204–4209. https://doi.org/10.1039/B704104G

18. Chung, K.-T. (2016). Azo dyes and human health: A review. *J Environ Sci Health C Environ Carcinog Ecotoxicol*, *34*(4), 233–261.

19. Coates, J. (2006). Interpretation of Infrared Spectra, A Practical Approach. In *Encyclopedia of Analytical Chemistry*. John Wiley & Sons, Ltd. https://doi.org/https://doi.org/10.1002/9780470027318.a5606

20. Correia, V. M., Stephenson, T., Judd, S. J. (1994). Characterisation of textile wastewaters - a review. *Environmental Technology*, *15*(10), 917–929. https://doi.org/10.1080/09593339409385500

21. Crini, G. (2006). Non-conventional low-cost adsorbents for dye removal: A review. *Bioresource Technology 97*(9), 1061–1085. https://doi.org/10.1016/j.biortech.2005.05.001

22. Crini, G., Lichtfouse, E. (2019). Advantages and disadvantages of techniques used for wastewater treatment. *Environmental Chemistry Letters 17*(1), 145–155. Springer Verlag. https://doi.org/10.1007/s10311-018-0785-9

23. Dampang, S., Purwanti, E., Destyorini, F., Kurniawan, S. B., Abdullah, S. R. S., Imron, M. F. (2021). Analysis of optimum temperature and calcination time in the production of cao using seashells waste as $CaCO_3$ source. *Journal of Ecological Engineering*, *22*(5), 221–228. https://doi.org/10.12911/22998993/135316

24. de Luna, M. D. G., Flores, E. D., Genuino, D. A. D., Futalan, C. M., Wan, M. W. (2013). Adsorption of Eriochrome Black T (EBT) dye using activated carbon prepared from waste rice hulls-Optimization, isotherm and kinetic studies. *Journal of the Taiwan Institute of Chemical Engineers*, *44*(4), 646–653. https://doi.org/10.1016/j.jtice.2013.01.010

25. Purnamasari, D. A., Nafisyah, L. S.Pi., M. Sc., Ph.D., A., Aprilianita Sari, S.Pi., M.Si, L. (2024). Innovative utilization of blood cockle shell waste (*Anadara granosa*) as a growth medium for *Nitzschia* sp. *Journal of Marine and Coastal Science*, *13*(3), 136–143. https://doi.org/10.20473/jmcs.v13i3.60239

26. Ellerbrock, R. H., Gerke, H. H. (2021). FTIR spectral band shifts explained by OM–cation interactions. *Journal of Plant Nutrition and Soil Science*, *184*(3), 388–397. https://doi.org/10.1002/jpln.202100056

27. Fan, B. Guo, Jia, L., Wang, Y. Lin, Zhao, R., Mei, X. Song, Liu, Y. Yan, Jin, Y. (2018). Study on adsorption mechanism and failure characteristics of CO_2 adsorption by potassium-based adsorbents with different supports. *Materials*, *11*(12). https://doi.org/10.3390/ma11122424

28. Foo, K. Y., Hameed, B. H. (2010). Insights into the modeling of adsorption isotherm systems. *Chemical Engineering Journal 156*(1), 2–10. https://doi.org/10.1016/j.cej.2009.09.013

29. Gupta, V. K., Suhas. (2009). Application of low-cost adsorbents for dye removal - A review. In *Journal of Environmental Management 90*(8), 2313–2342. Academic Press. https://doi.org/10.1016/j.jenvman.2008.11.017

30. Ha, S., Lee, J. W., Choi, S. H., Kim, S. H., Kim, K., Kim, Y. (2019). Calcination characteristics of oyster shells and their comparison with limestone from the perspective of waste recycling. *Journal of Material Cycles and Waste Management*, *21*(5), 1075–1084. https://doi.org/10.1007/s10163-019-00860-2

31. Hameed, B. H., Daud, F. B. M. (2008). Adsorption studies of basic dye on activated carbon derived from agricultural waste: *Hevea brasiliensis* seed coat. *Chemical Engineering Journal*, *139*(1), 48–55. https://doi.org/10.1016/j.cej.2007.07.089

32. Hart, A., Onyeaka, H. (2021). Eggshell and seashells biomaterials sorbent for carbon dioxide capture. *Carbon Capture*. IntechOpen. https://doi.org/10.5772/intechopen.93870

33. Heidarinejad, Z., Dehghani, M. H., Heidari, M., Javedan, G., Ali, I., Sillanpää, M. (2020). Methods for preparation and activation of activated carbon: a review. *Environmental Chemistry Letters 18*(2), 393–415. Springer Science and Business Media Deutschland GmbH. https://doi.org/10.1007/s10311-019-00955-0

34. Ho, Y. S., Mckay, G. (1999). Pseudo-second-order model for sorption processes. In *Process Biochemistry 34*.

35. Hu, X., Radosz, M., Cychosz, K. A., Thommes, M. (2011a). CO_2-Filling capacity and selectivity of carbon nanopores: Synthesis, texture, and pore-size distribution from quenched-solid density functional theory (QSDFT). *Environmental Science & Technology*, *45*(16), 7068–7074. https://doi.org/10.1021/es200782s

36. Ioannidou, O., Zabaniotou, A. (2007). Agricultural residues as precursors for activated carbon production-A review. *Renewable and Sustainable Energy Reviews 11*(9), 1966–2005. https://doi.org/10.1016/j.rser.2006.03.013

37. Islam, K. N., Ali, M. E., Bakar, M. Z. B. A., Loqman, M. Y., Islam, A., Islam, M. S., Rahman, M. M., Ullah, M. (2013). A novel catalytic method for the synthesis of spherical aragonite nanoparticles from cockle shells. *Powder Technology*, *246*, 434–440. https://doi.org/10.1016/j.powtec.2013.05.046

38. Istikharoh, I., & Bahtiar, R. (2022). *Analisis potensi ekonomi dan strategi pengelolaan limbah cangkang kerang hijau (perna Viridis) berkelanjutan (Studi Kasus: Desa Ketapang, Kecamatan Mauk, Kabupaten Tangerang)* (in Indonesian).

39. Iwanow, M., Gärtner, T., Sieber, V., König, B. (2020). Activated carbon as catalyst support: Precursors, preparation, modification and characterization. *Beilstein Journal of Organic Chemistry 16*, 1188–1202. Beilstein-Institut Zur Forderung der Chemischen Wissenschaften. https://doi.org/10.3762/bjoc.16.104

40. Janekarn, I., Hunt, A. J., Ngernyen, Y., Youngme, S., Supanchaiyamat, N. (2020). Graphitic mesoporous carbon-silica composites from low-value sugarcane by-products for the removal of toxic dyes from wastewaters: Carbon-silica composites for dye removal. *Royal Society Open Science*, *7*(9). https://doi.org/10.1098/rsos.200438

41. Kaewtrakulchai, N., Samattakarn, N., Chanpee, S., Assawasaengrat, P., Manatura, K., Wongrerkdee, S., Eiad-Ua, A. (2024). Solid shrimp waste derived nanoporous carbon as an alternative bio-sorbent for oxytetracycline removal from aquaculture wastewater. *Heliyon*, *10*(11). https://doi.org/10.1016/j.heliyon.2024.e32427

42. Kajjumba, G. W., Emik, S., Öngen, A., Kurtulus Özcan, H., Aydın, S. (2018). *Modelling of Adsorption Kinetic Processes-Errors, Theory and Application*. Intech Open.

43. Khan, M. M. A., Faheem, K., Anas, S., Kumar, M., Khan, A., Asiri, A. M. (2022). An overview of textile industry wastewater treatment using activated carbon catalysts derived from agricultural waste. In: M. Jawaid & A. Khan (Eds.), *Carbon Composite Catalysts: Preparation, Structural and Morphological Property and Applications* 407–423. Springer Nature Singapore. https://doi.org/10.1007/978-981-19-1750-9_11

44. Kurniawati, A., Hadi, S. P., Hidayat, J. W. (2023). *Pengelolaan Limbah Cangkang kerang Dengan Pendekatan Analisis Stakeholder (Studi Kasus: Desa Banyuurip, Mojoasem dan Ngawen, Kabupaten Gresik)* (in Indonesian).

45. Kwiatkowski, M., Fierro, V., Celzard, A. (2019). Confrontation of various adsorption models for assessing the porous structure of activated carbons. *Adsorption*, *25*(8), 1673–1682. https://doi.org/10.1007/s10450-019-00129-y

46. Li, Y. H., Wang, S., Luan, Z., Ding, J., Xu, C., Wu, D. (2003). Adsorption of cadmium(II) from aqueous solution by surface oxidized carbon nanotubes. *Carbon*, *41*(5), 1057–1062. https://doi.org/10.1016/S0008-6223(02)00440-2

47. Lim, S., Kim, J. H., Park, H., Kwak, C., Yang, J., Kim, J., Ryu, S. Y., Lee, J. (2021). Role of electrostatic interactions in the adsorption of dye molecules by Ti_3C_2-MXenes. *RSC Advances*, *11*(11), 6201–6211. https://doi.org/10.1039/d0ra10876f

48. Lima, É. C., Adebayo, M. A., Machado, F. M. (2015). Kinetic and Equilibrium Models of Adsorption. In C. P. Bergmann & F. M. Machado (Eds.), *Carbon Nanomaterials as Adsorbents for Environmental and Biological Applications* 33–69. Springer International Publishing. https://doi.org/10.1007/978-3-319-18875-1_3

49. Liu, S., Peng, Y., Chen, J., Yan, T., Zhang, Y., Liu, J., Li, J. (2020). A new insight into adsorption state and mechanism of adsorbates in porous materials. *Journal of Hazardous Materials*, *382*. https://doi.org/10.1016/j.jhazmat.2019.121103

50. Lua, A. C., Yang, T. (2004). Effect of activation temperature on the textural and chemical properties of potassium hydroxide activated carbon prepared from pistachio-nut shell. *Journal of Colloid and Interface Science*, *274*(2), 594–601. https://doi.org/10.1016/j.jcis.2003.10.001

51. Hubbe, M. A., Azizian, S., Douven, S. (2019). Implications of apparent pseudo-second-order adsorption kinetics onto cellulosic materials: A review. *BioResources*, *14*, 7582–7626.

52. Martinez, J., Wardini, J. L., Zheng, X., Moghimi, L., Rakowsky, J., Means, J., Guo, H., Kuzmenko, I., Ilavsky, J., Zhang, F., Dholabhai, P. P., Dresselhaus-Marais, L., Bowman, W. J. (2024). Precision calcination mechanism of $CaCO_3$ to high-porosity nanoscale CaO CO_2 sorbent revealed by direct in situ observations. *Advanced Materials Interfaces*, *11*(14). https://doi.org/10.1002/admi.202300811

53. Nasron, N.A., Azman, N. S., Rashid, S. S. M. N., Said, N. R. (2018). Degradation of Congo Red dye in aqueous solution by using advance oxidation processes. *Journal of Academia UiTM Negeri Sembilan*, *6*, 1–11.

54. Colthup, N. B., Daly, L. H., Wiberley, S. E. (1990). *Introduction to Infrared and Raman Spectroscopy* (Third Edition). Elsevier Inc.

55. Oral, Ç. M., Çalışkan, A., Göçtü, Y., Kapusuz, D., Ercan, B. (2020). Synthesis of calcium carbonate microspheres via inert gas bubbling for orthopedic applications. *Ceramics International*, *46*(3), 3513–3522. https://doi.org/10.1016/j.ceramint.2019.10.066

56. Ramirez, N., Sardella, F., Deiana, C., Schlosser, A., Müller, D., Kißling, P. A., Klepzig, L. F., Bigall, N. C. (2020). Capacitive behavior of activated carbons obtained from coffee husk. *RSC Advances*, *10*(62), 38097–38106. https://doi.org/10.1039/d0ra06206e

57. Sajjadi, B., Chen, W.-Y., Egiebor, N. O. (2019). A comprehensive review on physical activation of biochar for energy and environmental applications. *Reviews in Chemical Engineering*, *35*(6), 735–776. https://doi.org/doi:10.1515/revce-2017-0113

58. Sevilla, M., Fuertes, A. B. (2011). Sustainable porous carbons with a superior performance for CO_2 capture. *Energy Environ. Sci.*, *4*(5), 1765.

59. Sime, T., Fito, J., Nkambule, T. T. I., Temesgen, Y., Sergawie, A. (2023). Adsorption of Congo Red from textile wastewater using activated carbon developed from corn cobs: the studies of isotherms and kinetics. *Chemistry Africa*, *6*(2), 667–682. https://doi.org/10.1007/s42250-022-00583-2

60. Tan, I. A. W., Ahmad, A. L., Hameed, B. H. (2008).

Adsorption of basic dye on high-surface-area activated carbon prepared from coconut husk: Equilibrium, kinetic and thermodynamic studies. *Journal of Hazardous Materials*, *154*(1–3), 337–346. https://doi.org/10.1016/j.jhazmat.2007.10.031

61. Tan, X., Liu, Y., Zeng, G., Wang, X., Hu, X., Gu, Y., Yang, Z. (2015). Application of biochar for the removal of pollutants from aqueous solutions. In *Chemosphere 125*, 70–85. Elsevier Ltd. https://doi.org/10.1016/j.chemosphere.2014.12.058

62. Thommes, M., Kaneko, K., Neimark, A. V., Olivier, J. P., Rodriguez-Reinoso, F., Rouquerol, J., Sing, K. S. W. (2015). Physisorption of gases, with special reference to the evaluation of surface area and pore size distribution (IUPAC Technical Report). *Pure and Applied Chemistry*, *87*(9–10), 1051–1069. https://doi.org/10.1515/pac-2014-1117

63. Sigfusson, T., Leeper, A., Jégousse, C. (2024, April). *Zero Waste In The Seafood Industry*.

64. UNESCO Intangible Cultural Heritage. (n.d.). *Indonesian Batik*.

65. Vilén, A., Laurell, P., Vahala, R. (2022). Comparative life cycle assessment of activated carbon production from various raw materials. *Journal of Environmental Management*, *324*. https://doi.org/10.1016/j.jenvman.2022.116356

66. Wang, A., Liu, C., Ge, X., Meng, W., Pi, Y., Liu, C. (2021). Enhanced removal of Congo red dye from aqueous solution by surface modified activated carbon with bacteria. *Journal of Applied Microbiology*, *131*(5), 2270–2279. https://doi.org/10.1111/jam.15100

67. Wang, J., Guo, X. (2020). Adsorption kinetic models: Physical meanings, applications, and solving methods. *Journal of Hazardous Materials* 390. Elsevier B.V. https://doi.org/10.1016/j.jhazmat.2020.122156

68. Wu, F. C., Tseng, R. L., Huang, S. C., Juang, R. S. (2009). Characteristics of pseudo-second-order kinetic model for liquid-phase adsorption: A mini-review. *Chemical Engineering Journal 151*, 1–3, 1–9. https://doi.org/10.1016/j.cej.2009.02.024

69. Wulansarie, R., Rozaq, M., Bismo, S., Rengga, W. D. P. (2023). Degradation of Congo Red Dye in wastewater using ozonation method with $H2O_2$ catalyst. *Jurnal Ilmu Lingkungan*, *22*(1), 150–154. https://doi.org/10.14710/jil.22.1.150-154

70. Yoon, G.-L., Kim, B.-T., Kim, B.-O., Han, S.-H. (2023). Chemical-mechanical characteristics of crushed oyster-shell. *Waste Management*, *23*, 825–834. www.elsevier.com/locate/wasman

71. Zhang, J., Duan, C., Huang, X., Meng, M., Li, Y., Huang, H., Wang, H., Yan, M., Tang, X. (2024a). A review on research progress and prospects of agricultural waste-based activated carbon: preparation, application, and source of raw materials. *Journal of Materials Science 59*(13), 5271–5292. Springer. https://doi.org/10.1007/s10853-024-09526-3

72. Zhao, L., Fang, Y., Xu, X., Xu, J., Qin, S. (2021). Influence of calcination conditions on the adsorption properties of the wasted sea shell to the Dibutyl phthalate. *Global Nest Journal*, *23*(1), 137–142. https://doi.org/10.30955/gnj.003187

73. Zhu, Y., Li, Y., Ding, H., Lu, A., Li, Y., Wang, C. (2021). Multifactor-controlled mid-infrared spectral and emission characteristic of carbonate minerals ($MCO3$, M = Mg, Ca, Mn, Fe). *Physics and Chemistry of Minerals*, *48*(4). https://doi.org/10.1007/s00269-021-01140-y